

AFRL-SN-HS-TR- 2002-027

**NOVEL MATERIALS FOR OPTICAL
MEMORY/CORRELATOR SYSTEMS**

Dr. Selim Shahriar
Prof. Shaoul Ezekiel
MASSACHUSETTS INSTITUTE OF TECHNOLOGY
77 Massachusetts Avenue
Cambridge MA 02139

FINAL REPORT: APRIL 1999 – OCTOBER 2000

APPROVED FOR PUBLIC RELEASE



AIR FORCE RESEARCH LABORATORY
Sensors Directorate
80 Scott Dr
Hanscom AFB MA 01731-2909

20020729 115

TECHNICAL REPORT

Title: Novel Materials for Optical Memory/Correlator Systems

PUBLICATION REVIEW

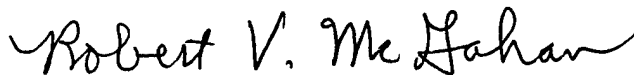
This report has been reviewed and is approved for publication:

APPROVED:



**CHARLES WOODS
AFRL/SNHC
Optoelectronic Technology Branch
Electromagnetics Technology Division**

APPROVED:



**ROBERT V. McGAHAN
Technical Advisor
Electromagnetics Technology Division**

ESC 02 - 0667

REPORT DOCUMENTATION PAGE			Form Approved OMB No. 0704-0188	
Public reporting burden for this collection of information is estimated to average 1 hour per response, including the time for reviewing instructions, searching existing data sources, gathering and maintaining the data needed, and completing and reviewing the collection of information. Send comments regarding this burden estimate or any other aspect of this collection of information, including suggestions for reducing this burden, to Washington Headquarters Services, Directorate for Information Operations and Reports, 1215 Jefferson Davis Highway, Suite 1204, Arlington, VA 22202-4302, and to the Office of Management and Budget, Paperwork Reduction Project (0704-0188), Washington, DC 20503.				
1. AGENCY USE ONLY (Leave blank)		2. REPORT DATE 6 June 2002		3. REPORT TYPE AND DATES COVERED FINAL 2 Apr 1999 - 2 Oct 2000
4. TITLE AND SUBTITLE Novel Materials for Optical Memory/Correlator Systems			5. FUNDING NUMBERS C - F19628-99-C-0016 PE - 61102F PR - SNH2689901009 PROJ - 2305 TA - DN WU - 02 Assec # DF300801	
6. AUTHOR(S) Dr. Selim Shahriar and Prof. Shaoul Ezekiel				
7. PERFORMING ORGANIZATION NAME(S) AND ADDRESS(ES) MIT 77 Massachusetts Avenue Cambridge, MA 02139			8. PERFORMING ORGANIZATION REPORT NUMBER	
9. SPONSORING/MONITORING AGENCY NAME(S) AND ADDRESS(ES) Charles Woods AFRL/SNHC 80 Scott Drive Hanscom AFB, MA 01731-2909			10. SPONSORING/MONITORING AGENCY REPORT NUMBER	
11. SUPPLEMENTARY NOTES				
12a. DISTRIBUTION AVAILABILITY STATEMENT Approved for public release; distribution unlimited.			12b. DISTRIBUTION CODE a	
13. ABSTRACT (Maximum 200 words) The objective of this project was to explore the characteristics of novel materials for optical data storage systems and correlators. To this end, we have made substantial progress.				
14. SUBJECT TERMS optical data storage systems correlators			15. NUMBER OF PAGES 17	
			16. PRICE CODE	
17. SECURITY CLASSIFICATION OF REPORT UNCLASSIFIED	18. SECURITY CLASSIFICATION OF THIS PAGE UNCLASSIFIED	19. SECURITY CLASSIFICATION OF ABSTRACT UNCLASSIFIED	20. LIMITATION OF ABSTRACT SAR	

1. INTRODUCTION

The objective of this project was to explore the characteristics of novel materials for optical data storage systems and correlators. To this end, we have made substantial progress. The technical achievements in this project are summarized below.

2. TECHNICAL ACHIEVEMENT

2.1 Observation and Study of Raman Excited Spin Alignment in NV-Diamond For Ultra-High Capacity Optical Memory

Recent developments in the field of quantum information and quantum computing has stimulated an intensive search for coherent physical processes which could be used to manipulate coupled quantum systems in a controlled fashion.[1] In this section, we describe our preliminary results demonstrating Raman excited spin alignment in NV-diamond, and its implication for the coherent generation and manipulation of entangled metastable states of interacting pairs of atoms. Our approach is based on the two-photon excitation of resonant transitions modified by a dipole-dipole interaction and presented in detail elsewhere. [2] Our existing sample 30 ppm NV-diamond was evaluated to be very promising for experimental realization of the proposed approach. In particular, optical transition at 637 nm has an inhomogeneous broadening of 750 GHz, and inhomogeneous width of 50 MHz. Considering required separation of 50 nm ($\lambda/12$), we have 900 coupled qubits per laser spot for sample with concentration of NV-centers of $5 \times 10^{18} \text{ cm}^{-3}$. For average spectral separation of 1.2 GHz (for atoms in $(\lambda/12)^3$ volume with existing concentration), magnetic field of less than 600 Gauss will be required to overlap transitions of adjacent atoms.

NV-diamond can be used also for high-temperature hole-burning memories. Optical spectral hole-burning has demonstrated the ability to achieve high-capacity, high-speed data storage [3]. The biggest stumbling block to its widespread application has been the requirement for low temperature operation and the associated costs thereof. To circumvent this problem, we have been investigating the possibility of using Raman excited spin coherences to store and recall optical data. The motivation is that optical Raman excitation allows storage densities and response times characteristic of optical hole-burning memories, but since it is based on long-lived spin coherences, it can maintain these characteristics at much higher operating temperatures. Proof-of-principle experiments have shown the ability to store and recall optical data using Raman excited spin echoes in Pr:YSO. The potential for higher temperature operation, without loss of performance, was also demonstrated in this material. Recently, we have shown that it is possible to observe Raman dark resonances above the spectral hole burning temperature in Pr:YSO. However, to achieve much higher temperature operation, a spectral hole-burning material with an allowed optical transition is required. This is necessary to offset the loss of efficiency of the Raman interaction, due to increasing optical homogeneous width as temperature is increased. For the initial experiments we chose to use N-V color

centers in diamond as the Raman hole-burning material because it is comparatively well studied [4].

The experimental setup used in the N-V diamond studies is shown in Figure 1. Here, a Raman enhanced non-degenerate four-wave mixing (NDFWM) technique is used to achieve a high signal to noise ratio, in analogy to experimental techniques used previously to study Pr:YSO [5]. In this scheme, coupling (C) and probe (P) field are used to write a grating in the ground state spin coherence via the resonance Raman interaction. This grating is read with a read beam (R) to produce a signal or diffracted beam (D). To further enhance signal to noise, a heterodyne detection scheme is used as shown in Figure 1(b). All dye laser beams are derived from a single dye laser output using acousto-optic frequency shifters. This greatly relaxes dye laser frequency stability requirements since the resonant Raman interaction is insensitive to correlated laser jitter. An additional beam from the argon laser (A) is also directed into the sample to serve as a repump. Without this repump beam, the N-V center would exhibit long-lived spectral hole-burning and no cw signal would be seen after a short time. The Raman transition frequency (~ 120 MHz) is determined by the spacing between the $S=0$ and $S=-1$ ground state spin sublevels. This spacing is controlled by applying a magnetic field of about 1 kGauss along the crystal (111) direction. At this field strength, the $S=0$ and $S=-1$ ground sublevels (for N-V centers aligned along (111)) are near an anti-crossing. These conditions are chosen to enhance Raman transition strength by compensating for the small spin-orbit coupling in diamond with a partial mixing the spin sublevels [4].

The observed NDFWM signal is shown in Figure 2 as a function of Raman detuning. For convenience, the Raman detuning is adjusted by tuning the spacing between the $S=0$ and $S=-1$ sublevels using the applied magnetic field. As shown, the Raman linewidth is about 20 MHz, which is comparable to the 15 MHz inhomogeneous width of the ground state spin transition. This width is significantly smaller than the homogeneous width (>25 MHz) of the optical transition and laser jitter (~ 100 MHz), and is taken as evidence of the Raman process. The asymmetry in the lineshape is due to interference with the (much broader) NDFWM signal at the anti-crossing. To eliminate this interference and to improve quality of the NDFWM signal, scanning of probe beam frequency is required. This was achieved by introducing electro-mechanical galvos. Compensating of angular displacement of coupling, probe, and reading beams, galvos allow scanning frequency of all beams. To further expand capability of the experimental setup, RF drivers for AOMs were configured to scan difference frequency between coupling and probe beam. A representative NDFWM signal obtained with modified setup is shown in Figure 3 as a function of frequency difference between coupling and probe beam. The value of the magnetic field was chosen about 1 kGauss and maintained constant.

Large optical matrix elements are required to maximize the number of gate operations per decoherence time. To evaluate matrix elements of our system, we investigated NDFWM diffraction amplitude as a function of laser intensity. The results are shown in Figure 4 for different laser intensities of coupling and probe beams. Intensity of the read beam was 25 W/cm^2 , and intensity of the repump beam was around 10 W/cm^2 . Saturation intensities

were found to be 5 W/cm^2 and 3 W/cm^2 for coupling and probe transition respectively. Relatively high values of saturation intensities might be explained high optical density of this particular sample. Using obtained values of optical matrix elements, we can expect 100-1000 logic gate operations per spin decoherence time.

It is interesting to note that laser intensity has a great influence not only on amplitude of the NDFWM signal, but also on symmetry of lineshape. Figure 5 illustrates observed this dramatic change in lineshape.

Trying to optimize experimental conditions for observation of NDFWM signal, we studied NDFWM signal lineshape as a function of applied magnetic field. The experimental results are shown in Figure 7. Sharp reduction in amplitude of the observed NDFWM signal far from central frequency most likely can be explained by limited bandwidth of the AOM used to scan the frequency of the probe beam. Further investigation of the obtained dependencies with proper renormalization of the signal is planned for the future.

Finally, Raman induced transparency of the probe field (P) has also been observed. Applying coupling laser power about 13 W/cm^2 , absorption suppression of the probe beam (1.3 W/cm^2) was evaluated to be about 4% (that corresponds change in transmission to be about 2.5%). Experimental traces are presented in Figure 8.

As a first step in investigation of spin echo in NV-diamond, we studied optical pumping effect on population of ground state. Regular NMR signal was detected at 430 MHz with applied magnetic field of 920 Gauss. RF power was modulated by square wave with frequency 50 Hz. Considering long lifetime of the metastable ground state, fall time of the observed pulses was strongly depended on efficiency of optical pumping. Experimental decay curve revealed two components: one weak component had constant fall time of about 5 ms, and the second stronger component had much shorter fall time, heavily depended on laser intensity. Therefore, weak component was attributed to unknown background signal, and the strong component was attributed to studied optical pumping effect. Experimental decay curves and corresponding fitting curves are shown in Figure 9.

Preliminary analysis of the NV-diamond showed a good potential of this material for experimental realization of solid state quantum computing based on dipole-dipole coupling. It was estimated, that existing sample can provide as many as 900 coupled qubits per laser spot for quantum computing in spectrally selective solids. Dark Raman resonances are observed and studied. Effects of laser power and magnetic field on Raman enhanced non-degenerate four-wave mixing signal are discussed. Optical matrix elements are found to be sufficient to allow 100-1000 logic gates operation per spin decoherence time. preliminary results on spin echo in NV-diamond are presented.

References

1. C. Williams and S. Clearwater, *Exploration in Quantum Computing* (Springer-Verlag, New York, 1998).
2. M.S. Shahriar, J. Bowers, S. Lloyd, and P.R. Hemmer, "Solid State Quantum Computing Using Spectral Hole Burning," submitted to *Nature*, and references therein.
3. H. Lin, T. Wang, and T. W. Mossberg, "Demonstration of 8-Gbit/in.² areal storage density based on swept-carrier frequency-selective optical memory," *Optics Letters* **20**, pp. 1658-1660 (1995); X. A. Shen, E. Chiang, and R. Kachru, "Time-domain holographic image storage," *Optics Letters* **19**, pp. 1246-1248 (1994)
4. X.F. He, N.B. Manson, P.T.H. Fisk, "Paramagnetic resonance of photoexcited N-V defects in diamond. I. Level anticrossing in the ³A ground state," *Physical Review B* **47**, 8809 (1993); A. Lenef, S. W. Brown, D. A. Redman, S. C. Rand, J. Shigley and E. Fritsch, "Electronic structure of the N-V center in diamond: Experiments," *Physical Review B* **53**, 13427-13440 (1996).
5. B. S. Ham, M. S. Shahriar, M. K. Kim and P. R. Hemmer, "Frequency-selective time-domain optical data storage by electromagnetically induced transparency in a rare-earth-doped solid," *Optics Letters* **22**, pp. 1849-1851 (1997).

Solid State Quantum Computing Using Spectral Hole Burning," M.S. Shahriar, J. Bowers, S. Lloyd, and P.R. Hemmer, submitted to *Nature*

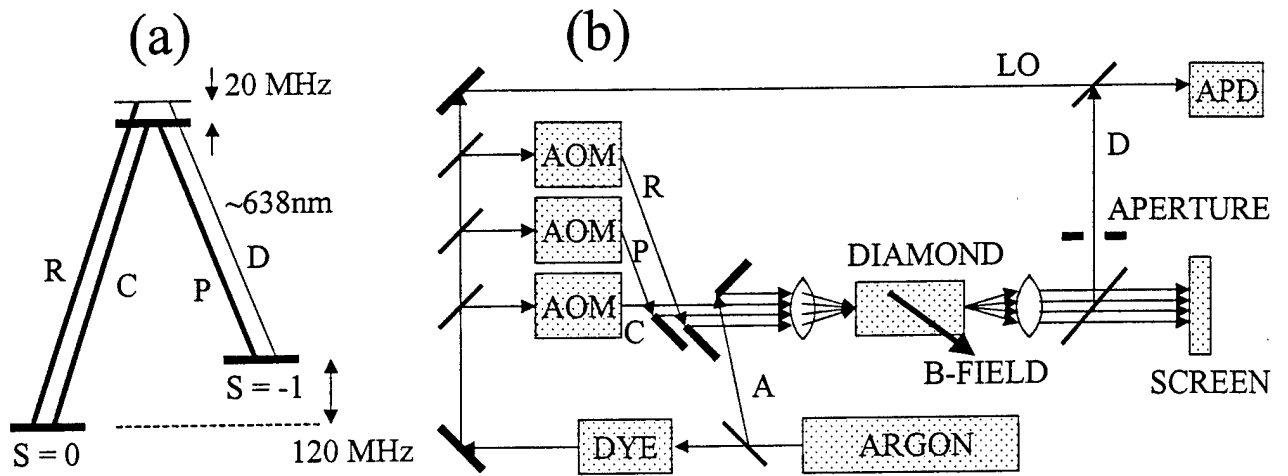


Figure 1. Experimental setup for observation of Raman excited spin coherences in N-V diamond. (a) Level diagram near anti-crossing. (b) Optical table setup.

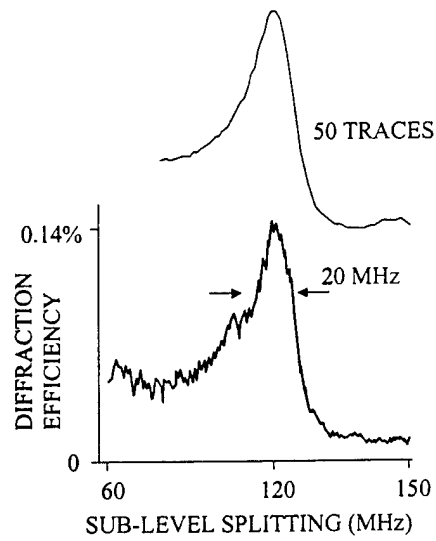


Figure 2. Raman enhanced non-degenerate four-wave mixing signal vs. magnetic field induced splitting of $S=0, -1$ states.

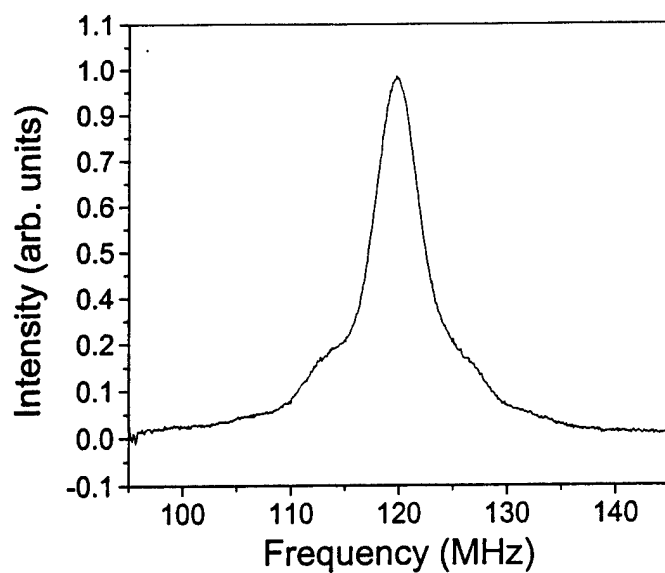


Figure 3. Raman enhanced non-degenerate four-wave mixing signal vs. frequency difference between coupling and probe beam.

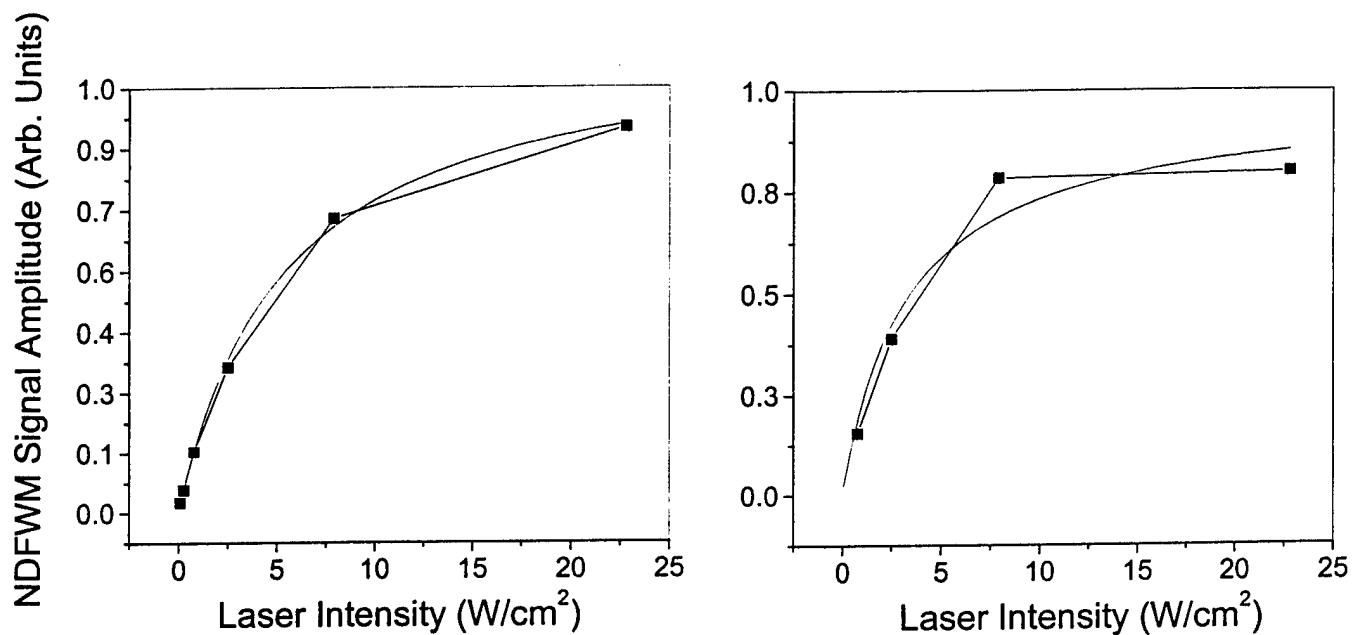


Figure 4. Amplitude of Raman enhanced non-degenerate four-wave mixing signal vs. laser intensity of coupling (left chart) and probe (right chart) beams.

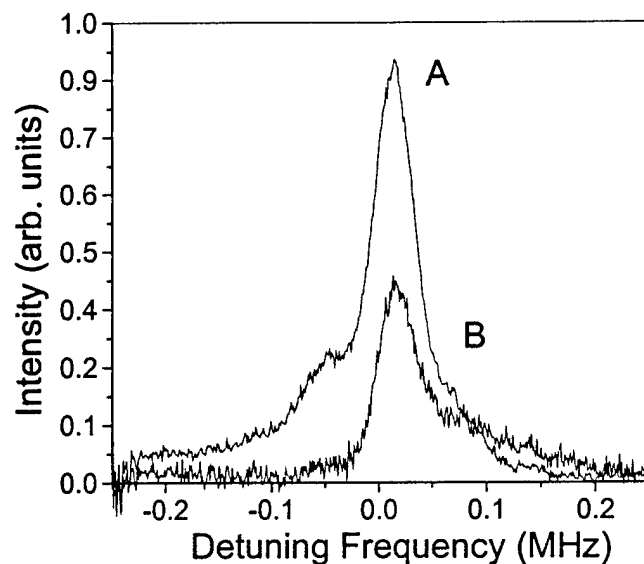


Figure 6. Observed raman enhanced non-degenerate four-wave mixing signal lineshape with applied full laser power (trace A) and 1/3 of full laser power (trace B).

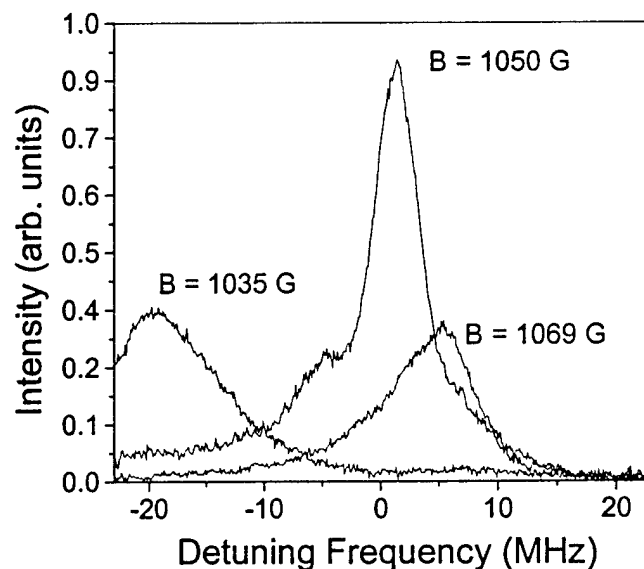


Figure 7. Raman enhanced non-degenerate four-wave mixing signal vs. magnetic field strength.

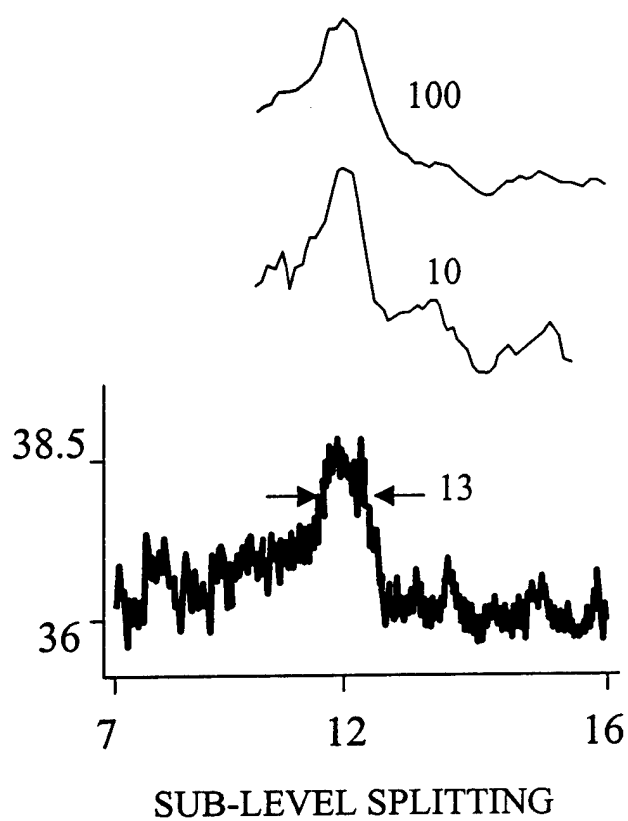


Figure 8. Absorption suppression in NV-diamond. Observed change in probe beam transmission is shown.

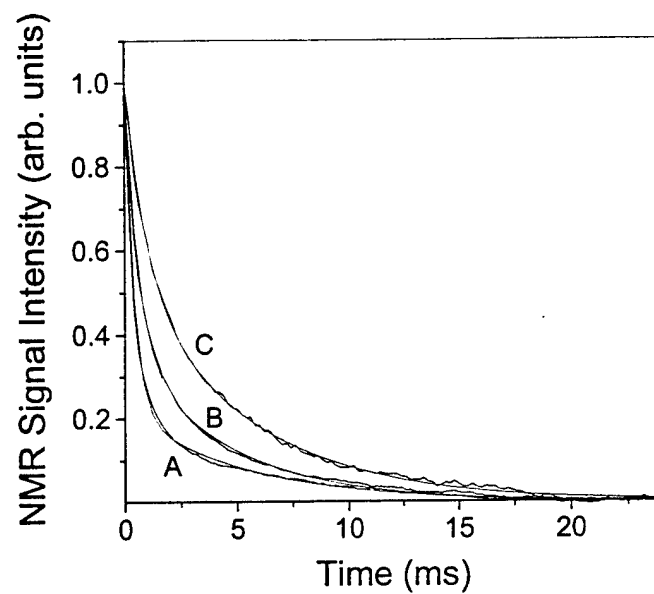


Figure 9. Ground state optical pumping after RF-pulse in NV-diamond. Optical pumping times of 0.40 ms, 0.58 ms, and 0.94 ms were found for laser powers of 96 mW/cm², 48 mW/cm², and 24

2.2 Automatic Target Recognition, Computer Vision, and Content-based Data Mining using Polymer-based Thick Holograms

We have been constructing a unit that will demonstrate rapid identification of a stored image via optical correlation. Briefly, we will store in an MMU (multiplexed memory unit) about a million (1,024,000, to be exact) images of various objects, viewed from different distances and perspectives. For our purposes, many copies of the same image would be used. We will then demonstrate that any one of these images can be identified via optical correlation with the stored images in the MMU.

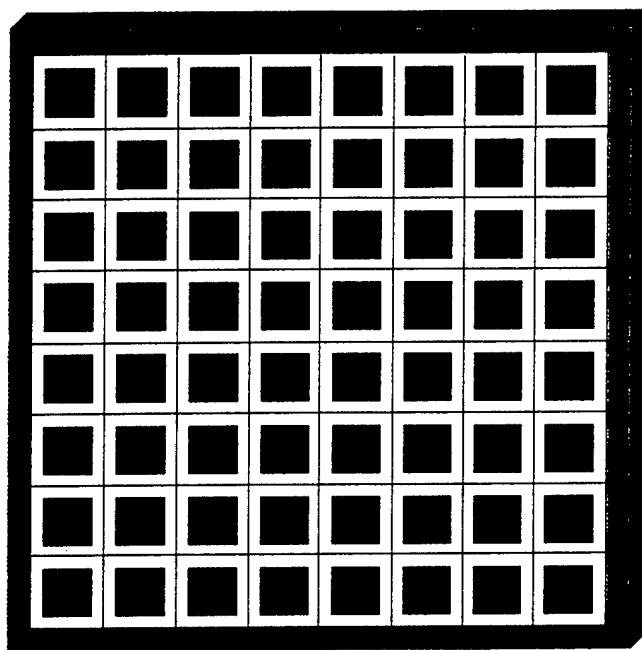


Figure 1: Schematic illustration of the Memplex Memory Unit, with a dimension of 124mm X 124mm X 2mm. The number of sub-units is 1600, although only 64 are shown for clarity. Each sub-unit has a dimension of 2mm X 2mm, and separated from one another by a 1 mm wide guard strip in all directions.

The MMU is shown schematically in figure 1. The sample will have a square dimension of 124 mm X 124 mm, with a 2 mm wide guard strip on each side. The active area of 120 mm X 120 mm will be sub-divided into smaller squares, each 3 mm X 3 mm,. This corresponds to a total of 1600 sub-divisions. The sub-divisions will be separated from one another by a 1 mm guard band on each side. This is necessary in order to allow the angular multiplexing.

The sample will have a thickness of 2 mm, corresponding to an angular selectivity of about 0.25 mrad, for a writing wavelength of 514.5 nm. We will use an angular separation of 0.5 mrad between each data page. At each subdivision, we will store 640 pages, corresponding to an angular spread of ± 9 degrees. The reference beam will be at an angle of 30° with respect to the normal to the sample. The image beams, corresponding to the 640 data pages, will span the range of -21° to -39° . This is illustrated in figure 2.

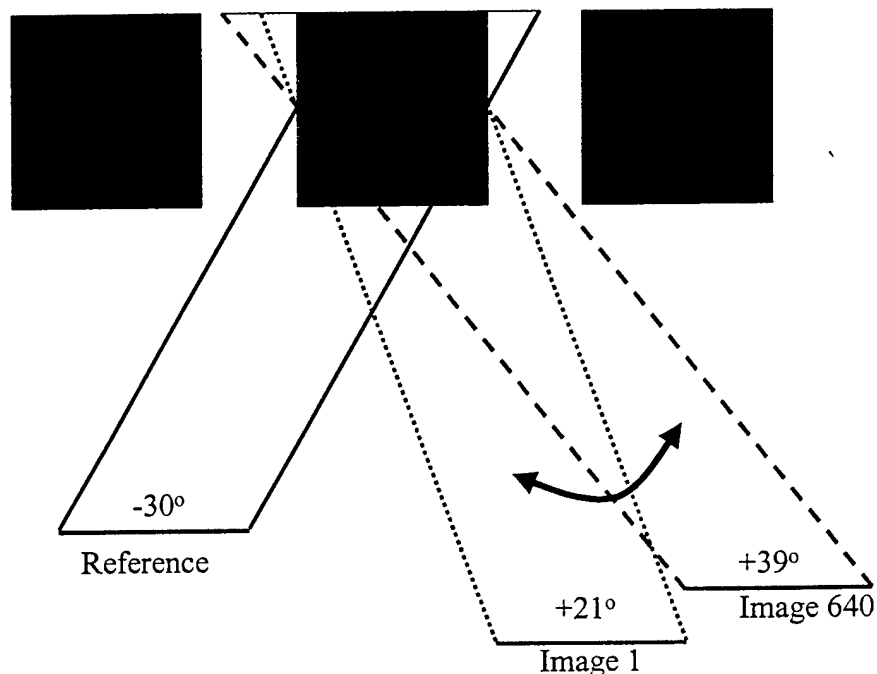


Figure 2: Schematic illustration of the angular multiplexing geometry, drawn to scale. The reference and image beams are incident on the MMU from the front. The reference beam is held fixed at -30° , while the image beam is scanned from $+21^\circ$ to $+39^\circ$, in increments of 0.5 mrad. Note that the 1 mm wide guard band is wide enough to eliminate potential cross-talks between neighboring sub-units.

Next, we discuss the 2D stage in some detail, as shown in figure 4. The assembly will consist of two different positioners. The MMU would be secured to the fine positioner (FP), and the FP would be secured to a coarse positioner (CP). Assume first that the CP has moved the sample to within 0.5 mm in both X and Y directions. The FP is then used to position the MMU precisely. This accomplished by using a feedback system. A diode laser is mounted at a position that remains fixed with respect to the writing apparatus. A screen, fastened to the FP, and parallel to the MMU, moves around in front of the diode laser as the FP moves the MMU. The surface of this screen (e.g. metal coated plastic) reflects the light back, which in turn is redirected to a photo-detector. This surface has a

number of holes, equaling the number of MMU sub-units, and separated from each other by the same distance as the MMU sub-units. The hole diameter is about 0.5 mm, while the laser beam diameter is about 1 mm. As such, the laser beam is aligned perfectly with the hole when the detector signal is minimized. A simple servo is used to guide the FP, first in the X direction, and then in the Y direction until this position is reached. Note

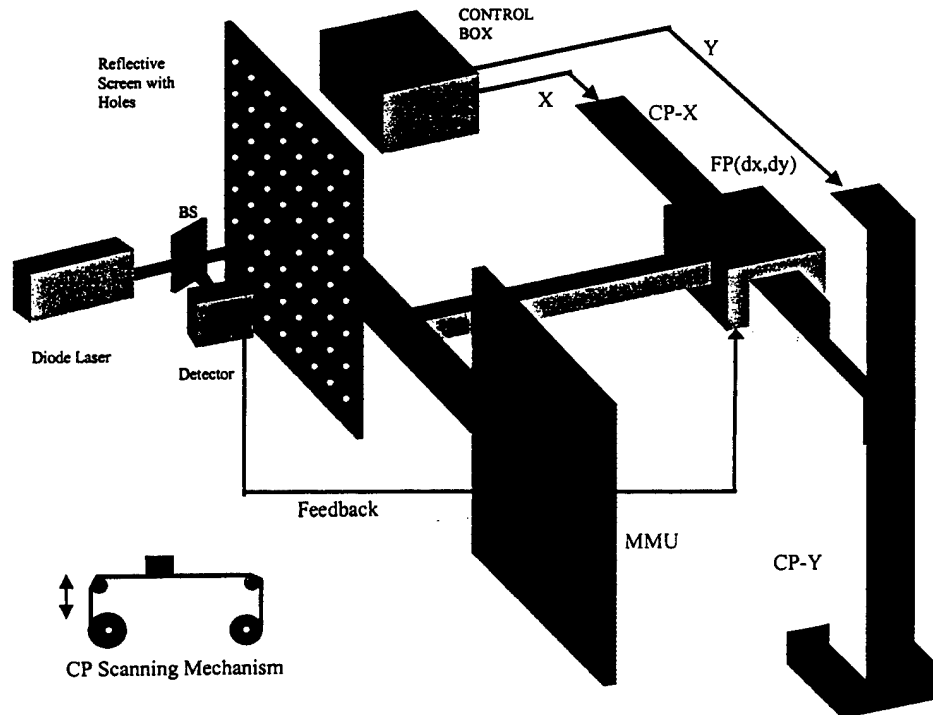


Figure 3. Schematic Illustration of the 2D scanning mechanism. See text for details.

that the MMU and the reference screen are mounted on a single bar, which in turn is connected to the FP. After the data has been stored, the MMU and the reference screen has to stay fastened to this bar at all times; otherwise, a painstaking (but not impossible) procedure has to followed to re-establish the one to one correspondence between the MMU sub-units and the holes in the reference screen.

The writing set up is illustrated in figure 4. We use a data base that we have developed containing pictures of military targets, including planes, tanks, armored vehicles and missiles. Altogether, we have put together a library of 2560 ($=4 \times 640$) images. Each image has been converted to a reduced image represented by 256×256 bits. This step is identical to what we had done in converting frames from a skating video during our earlier demonstration of holographic image storage and read-out. The reduced images will now be treated as the raw image files (RIF's). The RIF's will be named sequentially for automatic access, and be stored in a hard drive. We will store these 2560 images repeatedly 400 times to fill out the 1600 memory sub-units. For simplicity, the indexing information will be stored in a zip-drive disc. This disc will contain a set of files, representing a matrix of look-up tables, numbering a total of 1600 ($=40$ rows \times 40 columns). Each table will be in a separate file, and contain identification data for the images in each DS sub-unit. The files will be named such that the first two digits will represent the row number, and the second two digits will represent the column number. Table 1 below shows a sample of such files. After the first sub-unit is written to, the 2D-stage will be moved to the next sub-unit. Once four sub-units have been recorded, the process will be repeated, thus reusing the same set of images.

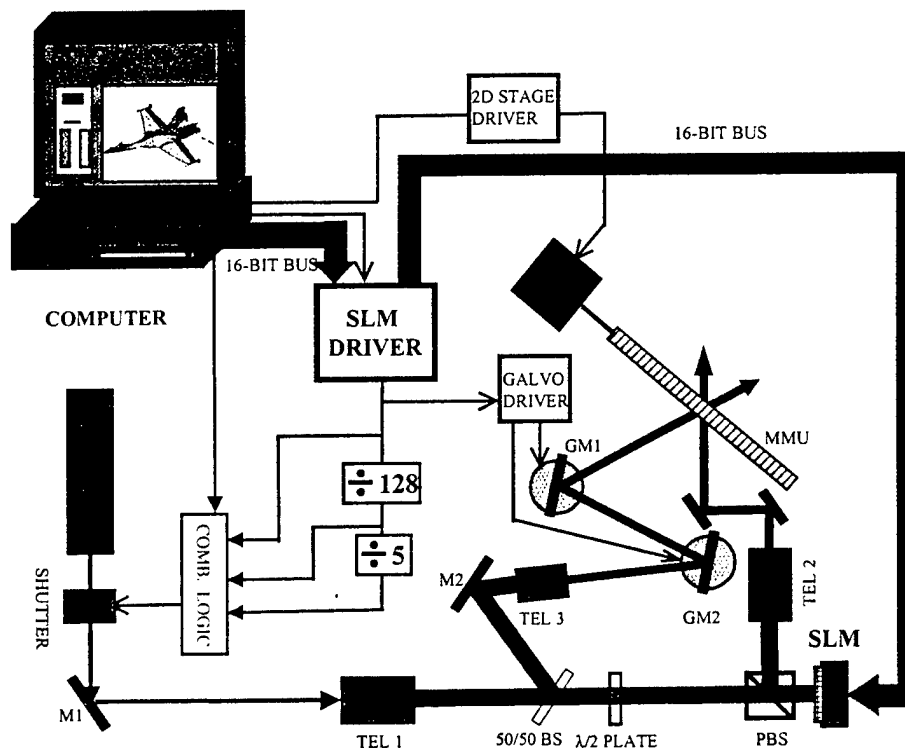


Figure 4. Schematic illustration of the writing set up for producing the image correlator. See text for details.

Table 1: A representative look-up table/file

File name: 2517 (row=25; column=17)				
<i>Image #</i>	<i>Object</i>	<i>Model</i>	<i>Distance(km)</i>	<i>Orientation(γ, ψ, ϕ)</i>
ooo	ooo	ooo	ooo	ooo
136	Plane	MIG 29	10	30, 0, 0
137	Plane	MIG 29	10	0, 30, 0
ooo	ooo	ooo	ooo	ooo
311	Plane	F16	4	0, 0, 0
312	Plane	F16	6	0, 0, 0
ooo	ooo	ooo	ooo	ooo
621	Plane	Tornado	2	15, 0, 30
622	Plane	Tornado	2	0, 0, 0
ooo	ooo	ooo	ooo	ooo

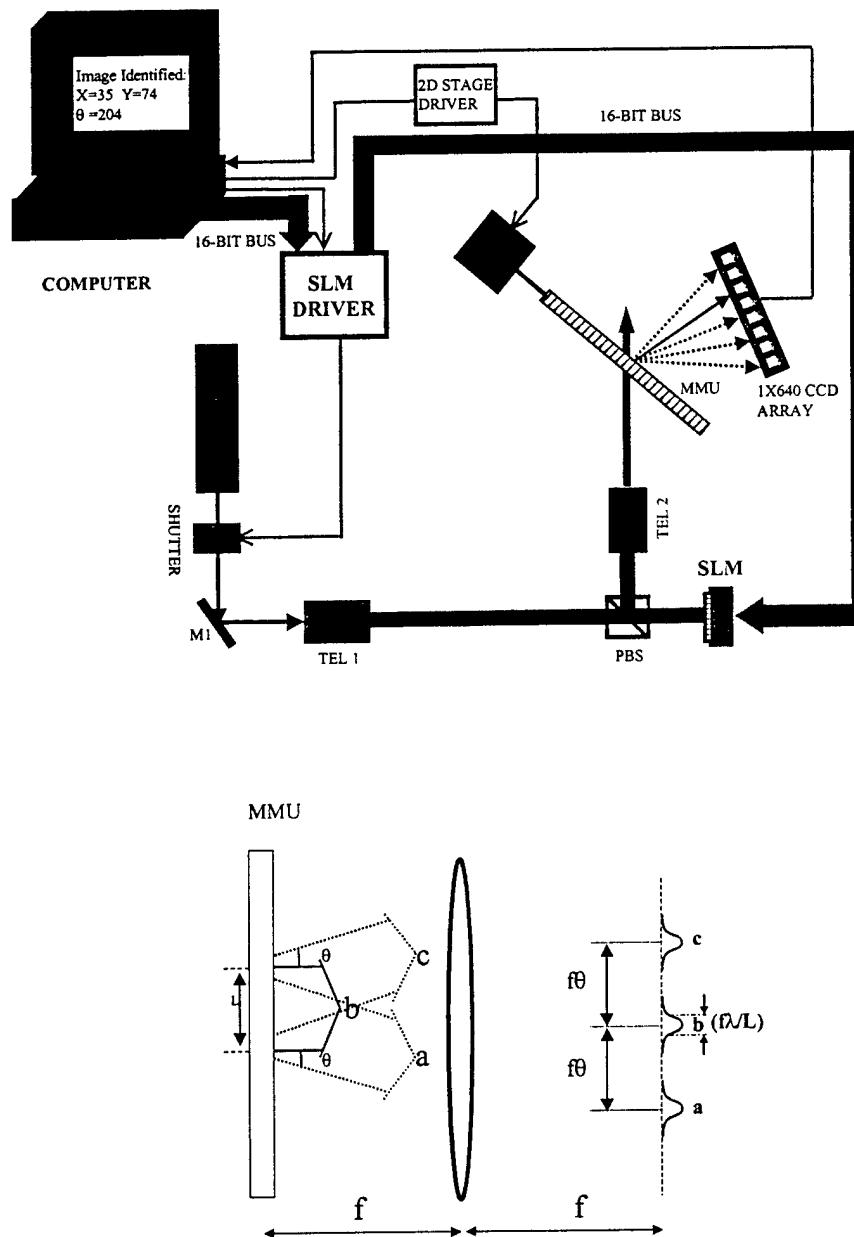


Figure 5. Top: Schematic illustration of the MMU based brass-board unit for image identification. Bottom: Lens to be inserted between the MMU and the CCD array in order to resolve the correlation spots. See text for details.

The reading process is illustrated in figure 5. The read-out is performed by a solid-state green laser (532 nm), with an output power of 20 mW. The output of this laser is passed through a shutter, and then expanded by a telescope (TEL1) to fill the area of the SLM.

To start with, the image in question is loaded into the SLM driver. The image reflected from the SLM is redirected by the polarizing beam splitter (PBS), and reduced in size (TEL2) to match the area of the memory sub-unit. To start with, the reference data file in the zip disc will be copied into the hard drive. As before, the whole reading/detection process will be controlled by a windows application program (WAP) written in C++. Once the user starts the program, the image in question will be loaded into the SLM driver. After the SLM driver has sent the image to the SLM, the shutter is opened, and kept on for a millisecond.

In order to detect a possible correlation peak, a linear ccd array is placed 10 cm behind the MMU. A lens of focal length 5 cm is placed between the MMU and the ccd array, as shown in the bottom of figure 6. Simple analysis then shows that the spots would be separated by a distance given approximately by $f\theta=25$ micron. The width of each spot is given approximately by $f\lambda/L$. The criterion for resolving the spots is then $L>\lambda/\theta$, which is clearly satisfied in our choice of parameters ($L=2$ mm, $\lambda/\theta\approx 1.06$ mm). Here we have assumed that the sidebands of the correlation peaks can be ignored; this can be guaranteed by making sure that the reference beams during the writing stage are not of square profile, but rather have Gaussian profiles. The ccd array consists of 640 elements, spaced 25 microns apart, in order to match the geometry chosen here.

Before the start of the query, the intensity of the read-out beam will be calibrated so that the correlation signal for a reference image produces an output voltage corresponding to a logic 1 for a TTL element. The 640 analog outputs will be loaded in parallel into a cascaded array of 20 shift-registers, each with 32 bits. Once the output signals are loaded into the registers, 640 cycles of a clock signal will be used to push the information out of the shift registers. The last (output) bit of the shift-register-cascade will be ANDed with a logic 1. The output of this AND gate will trigger the loading of a %640 counter (also driven by the same clock) into an 11 bit register, which in turn will be loaded into the computer through its parallel port. It is plausible that more than one correlation corresponding to a TTL logic 1 will occur. In this case, the power of the read-out beam will be reduced by a pre-determined amount, and the process repeated, until only one of the correlation peak registers as a logic 1. If no correlation occurs, the shutter is turned off, the 2D stage is moved to the next location, and the shift-registers are scanned again. This process is repeated through all the positions of the 2D Stage until a correlation peak is found. The WAP will then display the row and column numbers, and the image number, on the screen. In addition, it will retrieve the corresponding reference file, and display the vital information (e.g., name of the object, model number, distance and orientation --- see table 1) on the screen.

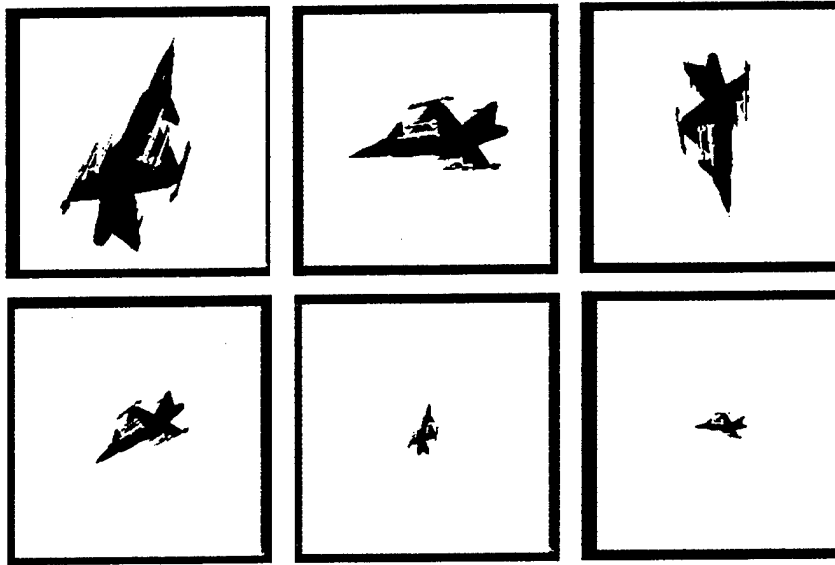


Figure 6: Different sizes and orientations of the same plane, recorded in a 256X256 bit grid. The correlator would be able to distinguish not only between different planes, but different orientations of the same plane.